Check for updates

AGU ADVANCING EARTH AND SPACE SCIENCE

Water Resources Research

RESEARCH ARTICLE
10.1029/2021WR031704

Analyzing Recharge Dynamics and Storage in a Thick, Karstic Vadose Zone

Patricia Spellman[1], Charles Breithaupt[1], Paul Bremner[2], Jason Gulley[1], John Jenson[3], and Mark Lander[3]

[1]School of Geosciences, University of South Florida, Tampa, FL, USA, [2]NASA Marshall Space Flight Center, Heliophysics and Planetary Science Branch, Huntsville, AL, USA, [3]Water and Environmental Research Institute (WERI) of the Pacific, University of Guam, Mangilao, Guam

Key Points:

- Vadose storage in eogenetic karst aquifers is appreciable, but most recharge typically occurs within a few months
- Our method can be applied to other areas where high-resolution data exists, as our results align with previous observations and models

Supporting Information:

Supporting Information may be found in the online version of this article.

Correspondence to:

P. Spellman,
pdspellm@usf.edu

Citation:

Spellman, P., Breithaupt, C., Bremner, P., Gulley, J., Jenson, J., & Lander, M. (2022). Analyzing recharge dynamics and storage in a thick, karstic vadose zone. *Water Resources Research*, *58*, e2021WR031704. https://doi.org/10.1029/2021WR031704

Received 2 DEC 2021
Accepted 6 JUN 2022

Author Contributions:

Conceptualization: Patricia Spellman
Data curation: Patricia Spellman
Formal analysis: Patricia Spellman, Charles Breithaupt, Paul Bremner
Funding acquisition: Jason Gulley
Investigation: Patricia Spellman
Methodology: Patricia Spellman, Charles Breithaupt, Paul Bremner
Resources: Jason Gulley, John Jenson, Mark Lander
Validation: Patricia Spellman
Visualization: Patricia Spellman
Writing – original draft: Patricia Spellman
Writing – review & editing: Charles Breithaupt, Paul Bremner, Jason Gulley, John Jenson, Mark Lander

© 2022. American Geophysical Union. All Rights Reserved.

Abstract Karst vadose zone heterogeneity creates complex transmission and storage dynamics that affect the timing and magnitude of aquifer recharge. Young, high-matrix permeability eogenetic karst aquifers may have significantly higher matrix storage than older, lower matrix permeability counterparts. In vulnerable and water-limited karst regions, the timescales of storage may be important for seasonal and sub-seasonal water resource management. We create a framework to quantify storage dynamics in karst aquifers using high-resolution precipitation and groundwater levels from the Northern Guam Lens Aquifer in the US territory of Guam. We estimate recharge using the Water Table Fluctuation method, and then develop transfer functions between precipitation and recharge to quantify storage and release of water from the vadose zone. The transfer functions are partitioned into different flow pathways including conduit, conduit/matrix, and slowly draining matrix. Probability distributions are fit to each pathway to determine the average travel times of infiltrated waters. The results show that aquifer recharge through secondary porosity features typically occurs within a few hours of a rainfall event, but this rapid recharge accounts for only 12%–28% of total recharge. The majority of aquifer recharge (>70%) occurs within a month of a contributing storm event. An additional 10% of recharge, on average, took longer than a month to reach the water table. The framework established can help improve the hydrological modeling and freshwater management for karst aquifers.

Plain Language Summary Recharge is a critical component of water resource allocation as it governs the availability of water for public, agricultural, and industrial supply. Therefore, understanding how precipitation becomes recharge to the aquifer is an important step in water resource management. However, in young, minimally evolved (eogenetic) karst that maintain significant primary porosity, appreciable vadose storage may occur. In island settings where water resources are volatile, the timing of precipitation to recharge significantly impacts groundwater stores and water resource allocation. We develop transfer functions between precipitation and recharge and use analytical methods to quantify (a) timescales of vadose storage, (b) estimates of storage and (c) magnitudes of recharge in a thick, karst vadose zone on Guam. Our work aligns with previous observations and provides a new method to estimate storage and transport through the vadose zone to karst aquifers.

1. Introduction

The volume and timing of groundwater recharge is fundamentally controlled by climate and to a lesser understood extent, the properties of the vadose zone. Climate governs the amount of water available for recharge, whereas the type, scale, and distribution of vadose zone porosity controls the rate of recharge by determining the transmission and storage properties. The rates of transmission and storage are further controlled by the thickness of the vadose zone and its permeability, and significant heterogeneity in vadose flow properties can induce highly variable storage times and transmission pathways. As the vadose zone processes can be complex, water resource management strategies commonly ignore vadose storage even in areas where storage may be appreciable (Ramon et al., 2007; Williams, 2008). Since vadose zone properties impose significant constraints on the rates and timing of recharge and storage, it is important to acknowledge and incorporate vadose dynamics in groundwater models and water resource management strategies, especially in water-scarce regions.

Characterizing vadose zone processes is particularly challenging in karst aquifers because of the significant karst vadose zone heterogeneity (Jukic & Jukic, 2004; Poulain et al., 2018). Karst aquifer vadose zones are characterized

by two dominant flow pathways; fast, preferential transmission through highly efficient solutional conduits, fractures, and faults (Ford & Williams, 2013; Jackson, 1997; Thrailkill, 1968; Veni, 1999; Williams, 2008) and slow, diffuse percolation through the intergranular/finely fissured matrix which can act as a storage reservoir (Breithaupt et al., 2021; Choquette & Pray, 1970; Florea & Vacher, 2006; Florea & Vacher, 2007; Moore et al., 2010; Vacher & Mylroie, 2002). However, depending on the diagenetic history of the system, the storage of the vadose zone can be highly variable (Vacher & Mylroie, 2002).

Two end-member classifications of karst based on the properties inherited from diagenetic history have been proposed: eogenetic and telogenetic (Vacher & Mylroie, 2002). Aquifer transmission and storage characteristics are the results of diagenetic histories, and can therefore be characterized in terms of this karst diagenetic classification. In telogenetic karst, which has experienced deep burial and uplift resulting in intergranular compaction and porosity occlusion, fast flow transmission is dominant over percolation and matrix storage in the vadose zone (Budd & Vacher, 1991; Ford & Williams, 2013). Repeated burial-compaction and uplift-unloading produces karst that is highly fractured with a low-permeability matrix. The hydrological consequence is that recharge, and subsequent groundwater flow, mostly occur through secondary porosity with limited flow and storage in the matrix (Florea & Vacher, 2005). Storage is thought to be concentrated in the highly weathered region closest to the surface called the epikarst (Williams, 2008). Epikarst is typically characterized by dense networks of solution-widened fissures that have higher effective porosities and transmissivities than the more massive limestone in the un-weathered vadose bedrock below (Ford & Williams, 2013). Spatial and temporal variability in cave drip waters has generally been attributed to the conductivity and storage properties of the overlying epikarst and vadose zone (Harmon, 1979; Smart & Friederich, 1986; Chapman et al., 1992; Padilla & Pulido-Bosch, 1995; Caballero et al., 1996; Kogov'sek 1997; Larocque et al., 1998; Batiot et al., 2003; Emblanch et al., 2003; Dyck et al., 2005; Panagopoulos & Lambrakis, 2006; Garry et al., 2008). Some recent work (Bautista et al., 2018), however, has documented the role of fracture distribution in the un-weathered vadose bedrock in controlling percolation rates. Other sources of storage include horizontally oriented cave passages, which can store appreciable quantities of water until a precipitation event occurs (Perrin et al., 2003).

A defining characteristic of eogenetic karst aquifers is their significant matrix porosity (up to ~40%) (Budd & Vacher, 1991). Eogenetic karst aquifers are geologically young and have not undergone significant burial or uplift. Thus, eogenetic systems retain matrix permeability typically orders of magnitude higher than telogenetic counterparts (Budd & Vacher, 1991). Because eogenetic karst has not had significant porosity reduction due to diagenetic alteration, it may behave similarly to the epikarst in telogenetic systems. Recent drip water studies in eogenetic systems show that continuous drip rates are commonly observed throughout the year, suggesting delayed storage even through the dry season (Bautista et al., 2018; Beddows & Mallon, 2018; Hernandez et al., 2019; Partin et al., 2012).

Regardless of diagenetic history, the complexities of storage and transmission dynamics in the karstic vadose zone have presented challenges in assessing water resources. On annual timescales, simple water budgets can effectively ignore storage, providing annual approximations of recharge and available water (Contractor & Jenson, 2000; Engott, 2011; Izuka et al., 2010; Jocson et al., 2002; Johnson, 2012; Jones et al., 2000; Vacher & Ayers, 1980; Vacher et al., 1990). However, significant sub-annual processes such as droughts and seasonal recharge thresholds (Jones et al., 2000), along with seasonal changes in vegetation growth and irrigation may need to be accounted for in aquifers with limited storage and high withdrawal, for which demand is usually highest when recharge rate is lowest. Finer temporal resolution budgets are commonly achieved by using numerical modeling methods that require pre-defining the structure of the vadose zone or making inferences on storage dynamics via parameterization. In aquifers with thick vadose zones, phreatic groundwater models that do not incorporate vadose dynamics cannot accurately replicate the timing and magnitude of seasonal changes in aquifer storage driven by seasonal changes in recharge (Jocson et al., 2002). Unfortunately, the complexity of numerical models generally precludes a stable coupling of vadose and phreatic processes. Recent innovative work by Habana et al., 2013 has applied classic reservoir models to simulate large-scale vadose dynamics in coupled vadose-phreatic models, but daunting challenges remain in developing models that can incorporate simultaneous, seasonal-resolution, fully coupled vadose-phreatic systems.

Transfer function models, however, can provide a means of characterizing vadose zone dynamics. Specifically, transfer function methods can quantify seasonally resolved relations between changes in recharge and changes in vadose transmission and storage in karst systems (Bailley-Comte et al., 2008; Besbes & De Marsily, 1984;

Padilla & Pulido-Bosch, 1995). Analyzing the transfer function characteristics via probability distribution fits can define the storage and release timescales (Godsey et al., 2010; Kirchner, 2005) of infiltrated water, thus providing detailed information of recharge dynamics. Transfer function models can be linked to numerical models to provide coupled models of vadose-phreatic dynamics.

We develop transfer function models to analyze vadose zone storage and recharge dynamics in a thick, karstic vadose zone on the US territory of Guam using high resolution groundwater and precipitation data. The karst aquifer on the US territory of Guam is a young, eogenetic karst aquifer that has appreciable matrix permeability and a deep vadose zone which ranges from 37 to 200 m thick. We adapt and develop time series analysis methods, to construct a template for recharge assessment in a highly fractured and heterogeneous vadose zone. We generate recharge time series using the Water Table Fluctuation (WTF) method using previously determined specific yields. The estimated recharge and precipitation time series are used to develop transfer functions between precipitation and recharge to (a) partition fast flow and diffuse percolation in the vadose zone and (b) estimate travel times via fitted probability distributions.

1.1. Study Site

Guam is a US Territory in the Western Pacific and is the southernmost island of the Mariana Island Arc. Guam is 544 km^2 in area and located 13.5°N. The total population on the island is 169,000 and the population is growing at a rate of 0.18% per year.

The island has two distinct physiographic regions, and each occupies almost exactly half of the island. Southern Guam is comprised of deeply weathered and deeply dissected Eocene through Miocene volcanic rocks, while the north is limestone plateau formed on uplifted Miocene through Pleistocene limestone underlain by Oligocene volcanic basement rocks (Tracy et al., 1959). The delineation between the north and south part of the island is marked by a fault that displaces the northern plateau by roughly 121 m. The faulting results in a sloping of the northern plateau to the south, whereby elevations of the northern tip of the island are 252 m, and in the southern part of the plateau are as low as 51 m (Figure 1) (Figure 2).

1.2. Hydrogeology and the Freshwater Lens

The primary freshwater resource on Guam is the freshwater lens that forms in the Northern Guam Lens Aquifer (NGLA), which consists of the northern limestone plateau (Figure 1) (Mink & Vacher, 1997). The NGLA supplies about 80% of the drinking water to the residents of Guam (Gingerich, 2013). The depth to the water table (or vadose zone), averaged over wet and dry seasons, ranges from 182 m on the northern plateau to a little over 30 m in the southern end of the limestone plateau. Where, the freshwater lens sits atop seawater, the groundwater is termed “basal” water, whereas when the groundwater sits on volcanic basement rock, it is termed “parabasal.” (Figure 1). Regardless of where the bottom of the freshwater lens rests, basal and parabasal water form a continuous groundwater system throughout the NGLA.

The NGLA is comprised of the Miocene through Pliocene Barrigada Limestone and the Pliocene through Pleistocene Mariana Limestone, which includes an argillaceous member next to the fault, and beneath the adjacent volcanic highland (Figure 1). The fine-grained detrital foraminiferal Barrigada Limestone makes up the core of aquifer, but is exposed on only 18% of the surface, where is otherwise covered and surrounded by the reef-to-lagoonal deposits of the Mariana Limestone. Estimated regional hydraulic conductivities of Barrigada Limestone have been as high as 15,240 m/d (Gingerich, 2013). The Mariana limestone on the coastal regions of the northern plateau has typically lower hydraulic conductivities (400 m/d–7,650 m/d). The Argillaceous Member of the Mariana Limestone makes up around 12% of the NGLA compared with its surface exposure. Hydraulic conductivities are low in the argillaceous, with estimates of between 3 and 8 m/d.

1.3. Climate

Guam's climate is tropical marine with average annual precipitation in the northern plateau of around 2,200 mm/yr and stable average daily temperatures of 27°C. Annual precipitation ranges from 1,600 mm/yr to 3,175 mm/yr. Average monthly temperature recorder at Apra Harbor has ranged from 26°C (January) to 28°C (June). Relative humidity during the day is around 65%–80% and 85%–100% at night. Guam has distinct wet and dry seasons.

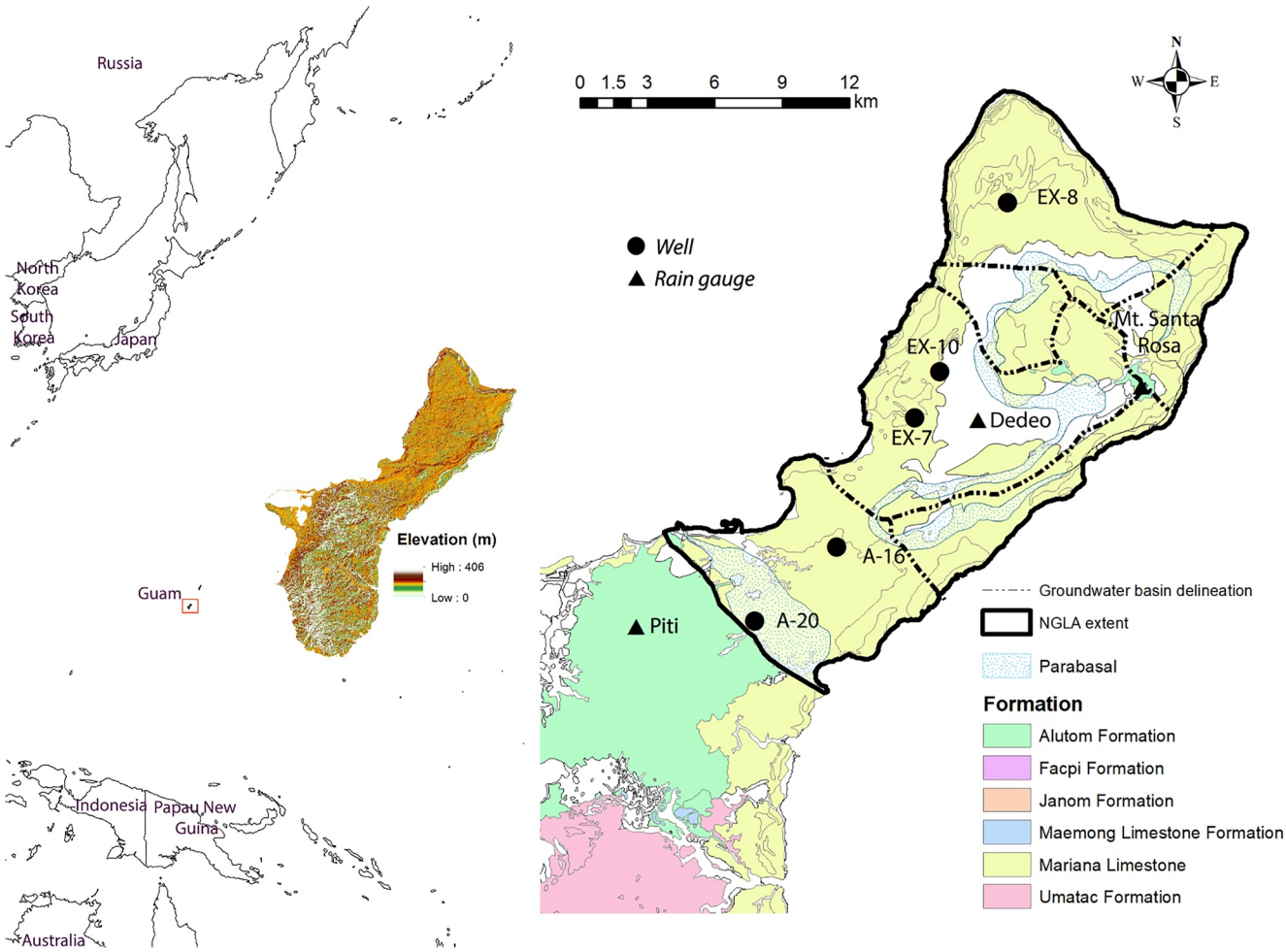

Figure 1. Locations of well and precipitation stations. Outline of northern Guam Lens Aquifer (NGLA) for the northern extent of the study region shown in hatched lines.

70 percent of the annual rainfall occurs in the wet season, which spans from June to November. The wet and dry seasons can produce significant differences in rainfall amounts per month. Average cumulative rainfall in the wet season is around 1,940 mm/season, whereas in the dry season it averages around 300 mm/season (Lander, 1994). Dripwater studies (Beal et al., 2019; Partin et al., 2012) using seasonal stable oxygen isotope signatures indicate that dry season rainfall makes no significant contribution to recharge.

Guam's climate is influenced by El Niño/La Niña oscillations which directly affect typhoon activity. El Niño/La Niña events are associated with changes in sea surface temperatures and atmospheric conditions between 5° N-5° S and 150°–90° W in the Pacific. During El Niño, when SST's are warmer than average, an increase in typhoon activity is generally observed. Additionally, increased SST's can drive wind patterns further increasing SST's and the potential for typhoon generation. The opposite occurs during La Niña, when SST's are lower than average, resulting in decreased typhoon activity. Typhoon generation does not necessarily mean Guam will be hit directly; rather, the risk of a direct hit increases during El Niño years. During the period of recorded typhoon activity, Guam has been impacted by 28 typhoons and numerous other tropical systems. Typically, drought conditions are observed after an El Niño year (Contractor & Jenson, 2000).

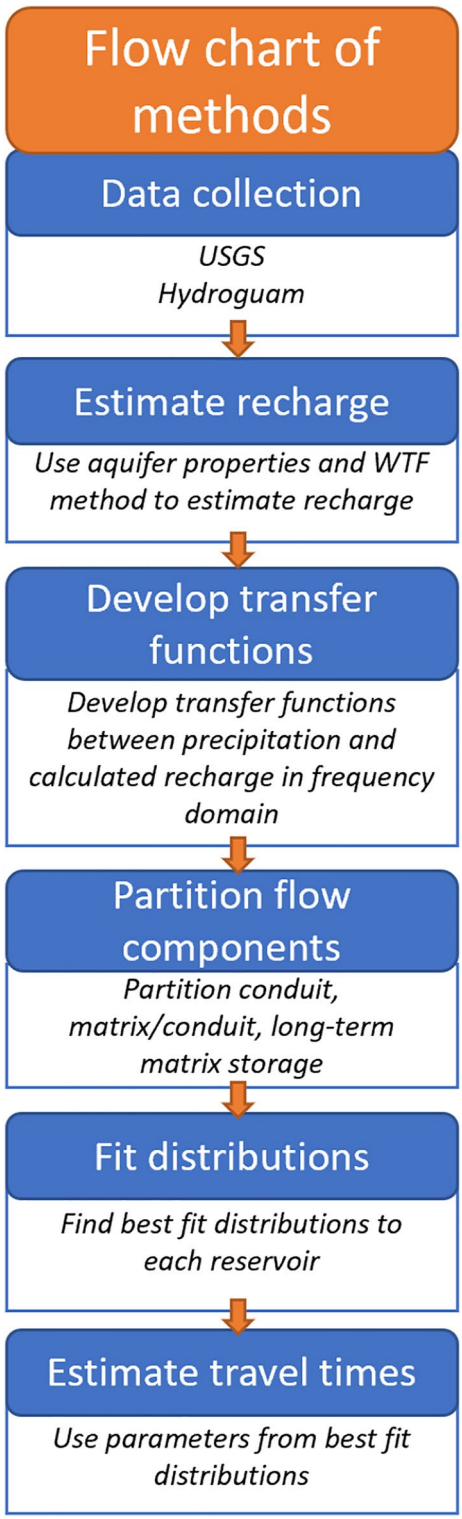

Figure 2. Flowchart showing methods described herein.

2. Methods

2.1. Data Collection

2.1.1. Groundwater Site Selection

A flowchart of the following methods is provided in Figure 2. Through a cooperative program with the University of Guam's Water and Environmental Research Institute of the Western Pacific the United States Geological Survey (USGS) has collected 10, 15, and 30-min groundwater level data for several observation wells, starting with water year 2007 (https://hi.water.usgs.gov/emaps/gwlevel-gu.html). We selected five wells that spanned a range of specific yields, hydraulic conductivities, and groundwater subbasins that also have overlapping, high resolution (sub-daily) continuous data. The final selection (Table 1) consisted of 5 wells and a time series of 2008–2012 (5 years).

In coastal and island aquifers such as the NGLA, ocean tides produce fluctuations in groundwater levels that needed to be removed to reveal the precipitation-induced signals. The extent of groundwater fluctuations from tides are a result of the hydraulic connectivity and distance to the ocean (Ferris, 1951). Numerous methods exist to remove the periodic tidal signal, whereby a Godin filter is recommended by the National Oceanic and Atmospheric Association (Pagendam & Percival, 2015; Shirahata et al., 2016; Walters & Heston, 1982). We therefore applied a Godin filter to the groundwater level data to smooth the signals using $N = 24$-point (for $\Delta t = 30$ min) window to remove the semi-diurnal tidal signal.

2.1.2. Climate Data

We obtained 30-min precipitation data from the USGS rain gages at Piti, Dededo, and Mt. Santa Rosa (Figure 1) 2008–2012. We gap-filled missing precipitation using data from the closest station via a linear regression. The technique was only necessary and applied for a month of missing data at Dededo in October 2009. If both stations had missing data, those data were considered zero values, however there were only 10 days where this was assumed reasonable. We used the closest precipitation station to a selected well for transfer function development.

2.2. Estimating Groundwater Recharge

2.2.1. Criteria for Selecting Best Method to Assess Recharge

Several methods exist for quantifying recharge to unconfined aquifers. Water balance methods are widely used at annual timescales, however, the WTF method is more reliable on shorter timescales (Healy & Cook, 2002). The WTF method is particularly suited for aquifers where groundwater response is rapid, such as in fractured media (Abusaada, 2019; Risser et al., 2005). Recharge calculations using the WTF method typically involve quantifying recharge at discrete time points of a captured recharge event, however a continuous time form of recharge estimation also exists (Crosbie et al., 2005). The continuous time method of recharge is estimated by taking the difference (ΔH) between the expected groundwater elevation had there been no recharge (H_t) to the observed head H_0 at that time step. The difference is multiplied by the specific yield (S_y) of the aquifer unit to obtain a time series of recharge (R_t) (Equation 1).

Table 1
Hydraulic Parameters (Rotzell et al., 2013) of Each Well Along With Vadose Thickness

Well	Specific yield	Average vadose thickness (m)	Hydraulic conductivity (m/day)
A20	0.005	37	8
A16	0.05	70	548
EX7	0.05	149	14,935
EX8	0.05	180	14,935
EX10	0.05	162	14,935

$$R_t = \begin{cases} S_y \Delta H & \text{if } H_t - H_0 > 0 \\ 0 & \text{otherwise} \end{cases} \quad (1)$$

To find the expected groundwater elevation without recharge, master recession curves (MRC) are fit to well hydrograph recessions. The MRC is defined by the function that best fits the shape of this recession curve and are commonly exponential functions (Equation 2) (Bailley-Comte et al., 2008; Healy & Cook, 2002; Maillet, 1905), although other functional forms can be used (e.g., polynomial, logarithmic, power). For this study we use the exponential function (Equation 2) to explain spring hydrograph recessions and thus storage release in karst aquifers, as it is the most commonly used in karst systems and is found to accurately represent karst recessions (Bailley-Comte et al., 2010; Bonacci, 1993; Ford & Williams, 2013). The exponential equation is expressed as

$$H_t = H_o e^{-kt}, \quad (2)$$

where H_t is the water level at time t, H_o is the initial water level and k (t^{-1} *units*) is the recession constant whereby $k = 1/\tau$, and τ is the mean residence time. We fit the MRC using least squares (LSQ) solution methods. The LSQ solution method involves first taking the natural log transform (Equation 3) of each side of Equation 2, to minimize Equation 4 and solve for k.

$$\ln(H_t) = \ln(H_o) - kt \quad (3)$$

$$\sum_{t=1}^{n} H_t(\ln(H_t) - \exp(H_o) - kt)^2 = 0 \quad (4)$$

Once the constants for the MRC are fit, the equation is used to predict water level (H_t) at time t. The difference between measured water level (H_o) and the predicted water level using Equation 2 results in ΔH which is multiplied by the specific yield (Equation 1). We used specific yields previously estimated using tidal signals by Rotzoll et al., 2013 using the same wells (Table 1). The specific yields estimated by Rotzoll et al., 2013 were later verified and used in a groundwater model for the NGLA (Gingerich, 2013) and thus we felt there was no need to estimate them again.

Typically, more than one recession is used to get a suite of recession constants (k) to ensure a stable, average value of k is obtained and to capture variability in storage and seasonal differences (Toebes & Strang, 1964). We estimated parameters of the MRC using recessions that lasted *at least* 15 days and had minimal events between peak to recession. We extracted all recessions meeting these criteria and calculated parameters of MRC using least-squares (LSQ) estimation (Equation 4). The mean and variance of the MRC coefficients (k) were taken and the mean value was used to calculate the water level for continuous recession.

2.2.2. Assumptions of WTF Method

The WTF method assumes that all water table increases are due solely to recharge and that specific yield is temporally constant. Avoiding wells that are impacted by storm water drainage reduces potential errors in recharge estimates, which were screened for in this analysis. The assumption of temporally constant specific yield can be a reasonable approximation in some hydrogeologic settings, though it can also lead to erroneous recharge estimates in karst aquifers (Worthington, 2019) or other highly heterogeneous aquifer systems.

We constrained error for recharge using ranges in effective porosity values from cores collected above and below the water table (Rotzoll et al., 2013). Typically, effective porosity is typically directly proportional to specific yields and was available at different vertical elevations within the vadose zone providing some grounding for error estimation in recharge. The average porosity above the water table was 13% whereas the average porosity below the water table was 21%. Given the estimated average porosity of 17%, and the 4% difference between 17%

and the upper (21%) and lower (13%) bounds, a 25% uncertainty value was used to constrain potential variability of recharge in each well.

2.2.3. Vadose Zone Dynamics

We determined travel times through the vadose zone using transfer functions estimated in the frequency domain between precipitation and recharge. Conversion from the time domain to the frequency domain was done using a Fourier transform (Molenat et al., 1999). Taking the Fourier transform and applying spectral analysis allows for a simplified assessment of complex processes at high resolution timescales that are difficult to parse and understand using traditional time series methods.

2.2.4. Estimating Power Spectral Density

The Fourier transform (Equation 5) is used to decompose complex signals in the time domain into their constituent frequencies.

$$F(\omega) = \int_{-\infty}^{\infty} f(t) e^{-i\omega t} dt \tag{5}$$

The power spectral density (PSD), which defines the estimated density of the decomposed signal at discrete frequencies, is the Fourier transform of the autocorrelation function (Equation 6). The autocorrelation of a signal reveals the internal serial correlation with respect to time of a data series and provides insight into the degree of memory represented by the discrete time signal. Functionally, it is a correlation defined at k-specified time lags (Equation 7). Thus, the Fourier transform of the correlation coefficient reveals the internal structure of the time series data in the frequency domain. The PSD will have units of the power of the signal per unit frequency.

$$\varphi(\omega) = \int_{-\infty}^{\infty} R_{xx}(t) e^{-i\omega t} dt \tag{6}$$

$$R_{xx}(t) = \frac{\mathrm{Cov}\left[Z_t, Z_{t-k}\right]}{\sqrt{\mathrm{Var}\left[Z_{t-k}\right], \mathrm{Var}\left[Z_{t-k}\right]}} \tag{7}$$

Because the Fourier transform assumes that the signal repeats itself indefinitely, its application to finite time signals can result in a phenomenon known as spectral leakage (i.e., energy transfer). Spectral leakage occurs when finite signals are repeated and discontinuities at the joined ends of the repeated time series are decomposed in the Fourier transform and resulting in spectral peaks not actually present in the real data. Spectral leakage to other frequencies can cause bias in the signal and thus, selection of appropriate methods to handle any discontinuities are usually considered prior to signal transformation. The Multi-taper method is one of such methods known to stabilize variance and minimize spectral leakage (Bronez, 1992; Thomsen, 1982).

The multitaper method (MTM) is a convolution method which applies specific tapers, Sleppian tapers, to the time series prior to the application of the Fourier transform to smooth connecting edges of the signal (Prieto et al., 2007; Thomsen, 1982). Because Sleppian tapers are orthogonal to each other, each iteration of the MTM highlights different features when convolved with the time series. Multi-taper methods are nonparametric: a useful property when the signal contains continuous and discrete events as is assumed with groundwater data. We used MTM via the MATLAB function pmtm to estimate the PSD of recharge and precipitation data using the MTM. Due to the lack of a metric to determine the optimal number of tapers in our study, the selection of taper number was based on previous studies where 5 tapers effectively preserved the integrity of a high-resolution oceanic signal. The selection of bandwidth (nw) follows from the selection of the number of tapers, as once tapers are optimized, the bandwidth is determined as 2(nw) – 1 = K, where K is the number of tapers. Thus, the time-half bandwidth used in this analysis was 3.

2.2.5. Defining the Transfer Function

The transfer function of an assumed linear system defines how the output will respond for a given input frequency signal. Mathematically, the relationship between input and output of a linear system in the frequency domain is defined by the frequency response function ($|H(\omega)|$.

$$Z(\omega) = |H(\omega)|\, X(\omega) \tag{8}$$

From Equation 8, the transfer function in the frequency domain ($|H(\omega)|^2$) can be defined as the squared modulus of the frequency response function and related linearly to the PSD of each series (Equation 9). Therefore, the empirical estimate of the transfer function would be the rearrangement of Equation 9 to and result in the ratio of the PSD of output ($\varphi_{ZZ}(\omega)$) to input ($\varphi_{XX}(\omega)$) (Equation 10).

$$\varphi_{ZZ}(\omega) = |H(\omega)|^2 \varphi_{XX}(\omega) \tag{9}$$

$$|H(\omega)|^2 = \frac{\varphi_{ZZ}(\omega)}{\varphi_{XX}(\omega)} \tag{10}$$

The resulting transfer function is a continuous signal relaying the magnitude of recharge observed for a given frequency input of precipitation. Probability distributions are fit to each transfer function at each well for the partitioned flow regimes described hereafter.

2.2.6. Partitioning Different Flow Regimes Within the Vadose Zone

We partitioned the transfer functions into three different domains: conduit flow, combined matrix/conduit flow and slow matrix flow. The conduit only component is dominated by quick fracture and conduit recharge and is assumed to happen on the same timescales as precipitation, hence why we assume that fast flow routes would mimic that of the white noise precipitation signal. Matrix/conduit flow is defined as mostly matrix dominated flow, however with the assumption that some fast conduit or fracture flow may still be occurring. And finally, slow matrix only flow is the long-term storage component of flow that occurs on long timescales. The remaining text refers to these three components based on the aforementioned partitions.

We partitioned conduit flow from matrix/conduit flow and matrix/conduit flow to only matrix flow by using visual and mathematical methods. We first established a break in the flatline behavior of the conduit only domain by finding a divergence point between the white noise spectrum of precipitation and the transfer function. The Fourier transform of time series precipitation approximates white noise at sub-daily frequencies which has characteristics of a flat spectrogram with zero-autocorrelation (Vasseur & Yodzis, 2004). To find this break point, we discretized the frequency at intervals of 0.01 Hz and took the ratio of the mean of PSD of the transfer function assumed to be white noise and scaled it by the standard deviation (Supplemental). Thus, when following the direction from high to low frequency, the point when the PSD of the transfer function begins to diverge from a steady mean is taken as the point where recharge is no longer explained entirely by precipitation but rather by another process. We assumed this process to be water coming out of storage. The frequency that was identified was also confirmed visually by plotting a vertical line and by fitting a polynomial to the data set and identifying the frequency of the inflection point. The same concepts and methods were applied to find the break between matrix and matrix/conduit flow, however the break between matrix/conduit and matrix flow was approached from the lowest frequency when taking the mean and standard deviation (Supplemental).

2.2.7. Estimating Travel Times

Fitting probability distributions to the empirical transfer function (Equation 10) provides average travel times through each of the three partitioned components. There exists a wide range of probability distributions whose efficacy is determined by the process type one wishes to capture. In hydrological applications, several distributions are commonly used to quantify processes.

For conduit only (fast) flow, the assumption of a white noise process predicated normally (Gaussian) distributed data for the recharge and precipitation spectra. Therefore, the normal distribution (Equation 11) was fit to the transfer function that represented conduit only flow.

For the conduit/matrix and matrix only flow, two distributions were considered: exponential and gamma. For karst systems, the exponential distribution (Equation 12) is commonly used to characterize spring recession curves providing details about the storage capacity of a catchment via parameter estimation (Bonacci, 1988). The exponential distribution assumes a well-mixed reservoir with only a single parameter to quantify a decay rate. Exponential distributions have been well suited to simulate simple reservoir systems and several studies have used them to estimate travel time distributions in the vadose zone (Bonacci, 1993). The gamma distribution (Equation 13) is a derivative of the exponential distribution but has two parameters that can allow for more weight in the distribution tails which can more accurately capture the travel time dynamics of a heterogeneous system. The gamma distribution is related to a scaled, exponential limited power law. Therefore, initial values of the shape

parameter can be estimated by first deriving power law relationships. Quantitatively, the gamma distribution is the sum of exponential distributions (Pishro-Nik, H., 2016) and as such, represents the complexity of potentially multiple components or non-linear processes within a system.

$$f(x)^{\text{normal}} = \frac{1}{\sigma\sqrt{2\pi}} e^{\frac{-(x-\mu)^2}{2\sigma^2}} \tag{11}$$

$$f(x)^{\text{exp}} = \frac{1}{\theta} e^{--\frac{x}{\theta}} \tag{12}$$

$$f(x)^{\text{gam}} = \frac{x^{\alpha-1} e^{--\frac{x}{\theta}}}{\Gamma(\alpha)\theta^{\alpha}} \tag{13}$$

The Gaussian distribution parameters are well known: σ is the standard deviation and μ is the expected value or mean of the distribution. For the gamma distribution, θ is a scale parameter that defines the spread of the distribution and α is a shape parameter. For the gamma distribution the relationship between θ and α is $\theta = t_0/\alpha$ where t_0 is the mean travel time. The exponential distribution has the same scale parameter, θ, but lacks a shape parameter. Thus, the mean of the exponential distribution is $1/\theta$.

2.2.8. Parameter Estimation for Distributions

We determined best fit parameters for Gaussian, exponential and gamma distributions for each of the partitioned components by minimizing the sum of squares between the empirical transfer function (Equation 10) and the distribution for each of the functions derived for the frequency domain (Equations 14–16). Initial estimates for the shape parameter for the exponential and gamma distribution were obtained by fitting a power law function to the empirical transfer functions (Chen et al., 2002; Godsey et al., 2010; Kirchner & Neal, 2013). Using the power law slope parameter as initial values for the shape parameter, we used the MATLAB function **fminsearch** to minimize the sum of squares between empirical and theoretical distributions. The distribution characteristics were then used to estimate average, median and variance of water travel times in each of the partitioned components.

$$F(f) = e^{-2\pi^2 f^2 \sigma^2} \tag{14}$$

$$F(f) = \left(1 + 4\pi^2 f^2 \theta^2\right)^{-1} \tag{15}$$

$$F(f) = \left(1 + 16\pi^2 f^2 \theta^2\right)^{\alpha} \tag{16}$$

3. Results

3.1. Recharge Estimates Using WTF Method

After tidally filtering the data (Figure 3), point recharge at each well calculated from 2008 to 2012 was greater at the northern wells than in wells in the argillaceous (Table 2). Wells within the Barrigada limestone (EX-7, EX-8, EX-10) had the highest recharge, 46% of average annual rainfall (using 2,200 mm/yr). The A-20 well located in the argillaceous member of the Marianna limestone had the lowest recharge at about 4% of annual rainfall. Estimated recharge as a percentage of rainfall all fell within previous estimated values of recharge to the NGLA with the exception of low percentages at A-20.

3.2. Transfer Function and Distribution Fits

Distribution parameters and goodness of fit as mean squared error (MSE) are shown in Table 3. Mean squared error were reasonable for all three components across all wells as they were within the variance of each data set. Best fit distribution for the slow flow matrix component was a gamma distribution, and therefore parameter estimates for gamma are reported. Both gamma and exponential fits were attempted for the transition to long-term matrix storage, but the power law initially fit to the data showed the best fit based on MSE (Figure 4).

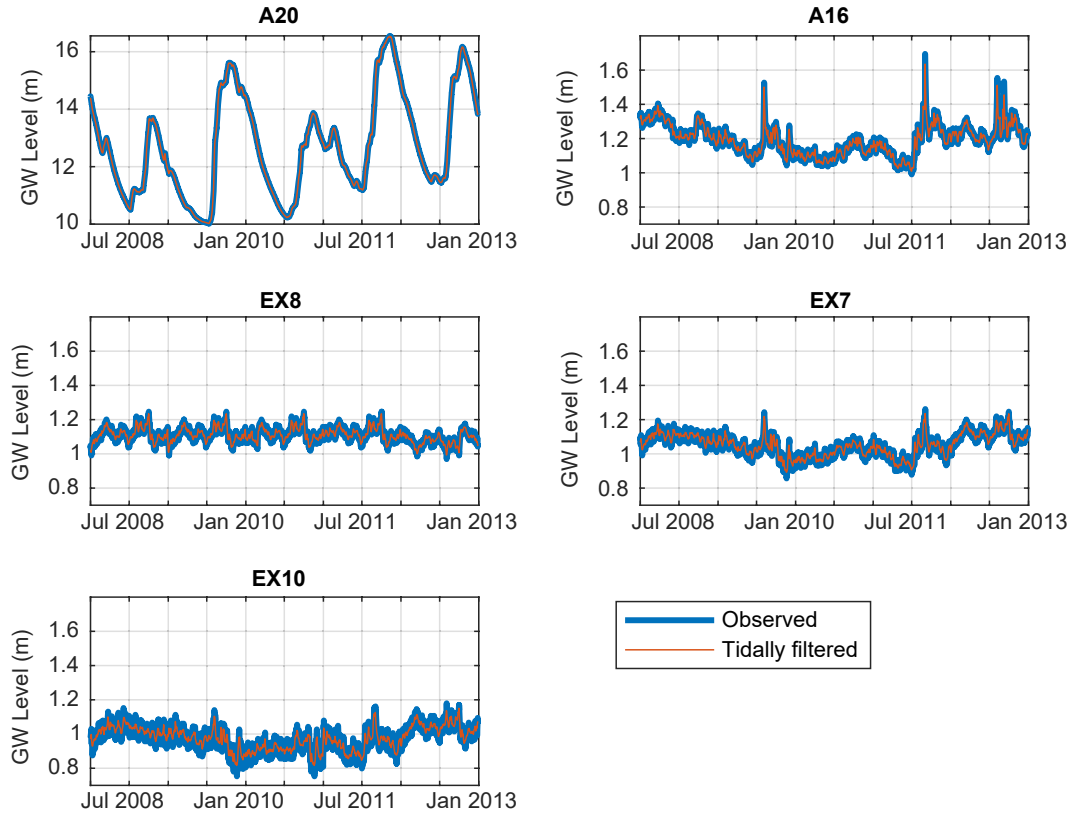

Figure 3. Water level and Godin filtered water level at each well. Axes on different scales for A-20 due to significantly more variability.

Using the parameter estimates from Table 3, travel times between each component were calculated. For conduit flow, mean travel times were 1.19 hr averaged over all sites. The highest frequency able to be resolved, the Nyquist frequency, is 1 hr, as the sampling interval was 30 min. Therefore, it is more accurate to say that conduit delivery of recharge to the water table happens rapidly, occurring *within* 1.5 hr of the onset of precipitation. Mean travel time through the transitional matrix/conduit component was 3.94 hr, with a lower bound of 1.75 hr at the matrix/conduit transition and upper bound of 21.15 days marking the transition to complete matrix flow. There is likely some fracture flow that occurs during matrix drainage, but the scaling behavior observed in the transfer function means that it is dominated by storage effects. The scaling behavior of the matrix/conduit flow shown in Figure 4 is representative of common $1/f^{\alpha}$ scaling behavior observed in other systems. The best fit of a gamma distribution thus highlights the higher density of travel times in the higher frequencies. Therefore, the shape parameter that can adjust for this density in the tails captured this trend and provided a better fit over the exponential for the transfer function across these frequencies. There is no finite mean associated with power laws where

Table 2
Annual Recharge Estimates With Error Bounds (25%)

Well	Average annual recharge (mm/yr)	Lower bound recharge (mm/yr)	Upper bound recharge (mm/yr)	Percent recharge of precipitation	Lower bound % recharge of precipitation	Upper bound % recharge of precipitation
A20	88.91	66.68	111.14	4%	3%	5%
A16	985.90	739.42	1,232.37	45%	34%	56%
EX7	998.40	748.80	1,248.00	45%	34%	57%
EX8	1,011.08	758.31	1,263.84	46%	34%	57%
EX10	1,009.49	757.12	1,261.86	46%	34%	57%

Table 3
Parameter Fits for Each Compartment Distribution

	Conduit			Matrix/conduit			Matrix	
Well	μ	σ	*MSE*	α	θ	*MSE*	α	*MSE*
A-20	69.85	2.28	1.67	1.66	0.35	7.60	0.14	10.36
A-16	74.93	4.17	1.60	0.80	0.18	7.06	0.14	9.74
EX-7	83.55	2.65	1.60	0.95	0.21	7.10	0.16	9.73
EX-8	68.24	1.34	1.44	0.95	0.26	6.03	0.18	8.80
EX-10	69.67	2.02	1.45	1.27	0.25	6.07	0.17	8.80

Note. A slope of 0 is assumed for conduit partition, but the matrix/conduit partition slope is obtained via alpha/theta.

scaling exponents are >-2, and as such, the median value for the longer-term matrix storage component is reported instead of the mean (Table 3). A power law fit indicates a heavy distribution tail (heavier than gamma) with greater than 80% of observations occurring in the tails.

Vadose zone storage is a significant component of recharge dynamics (Figure 5). For wells with lower permeability (A-20) and a thicker vadose zone (EX-7, EX-10), conduit contributions were smaller (12%–22%). The highest contribution of flow from conduit sources (28%) was EX-8 located in the northwestern part of the island. For all wells, most water (>70%) remained in storage and was slowly released over a period of a few weeks to months.

Volumes of water stored and released from vadose storage for the timescales analyzed highlight the significance of the storage in the vadose zone. An average of 12% of recharged water remained in vadose storage for longer than a month, eventually moving out of storage over several months. If the amount of recharge calculated is 46% of 2,200 mm/yr (1,012 mm/yr) and multiplied over the basins of the NGLA (ignoring basin representative of A-20), we obtain a volume of 216 km^3 of recharge to the NGLA. The volume that remains in long-term storage would then be 25 km^3 or 6.86×10^{12} gallons of water, representing 12% of the infiltrated water.

4. Discussion

Recharge estimates found in this study aligned well with other studies (Gingerich, 2013; Jocson et al., 2002; Johnson, 2012; Mink, 1976) providing confidence in the modeled storage and transmission characteristics of the vadose zone (e.g., Lander, 1994). The developed transfer functions showed distinctive scaling effects seen in modeling catchment dynamics (Kirchner et al., 2000), but the interpretation for vadose zone characteristics is different and discussed hereafter.

4.1. Recharge

We compared our recharge estimates to recharge values determined by other studies. Though constraining absolute magnitudes of recharge was not the primary goal of this analysis, it is important to validate against previous values because the time series of generated recharge impacts the overall transfer function and subsequent travel time distribution fits. Most estimates of recharge on Guam have shown recharge is between 39% and 67% of average annual rainfall (Gingerich, 2013; Jocson et al., 2002; Johnson, 2012; Mink, 1976). Our estimated recharge value of 46% of annual rainfall falls within those ranges except for the extreme southern well, A-20 (Table 2).

High recharge rates in northern Guam are facilitated by high matrix porosity and abundant karstic vadose fast flow routes characteristic of the pure carbonate bedrock. Lower recharge in the southern part of the lens is likely due to clay layers interbedded within the argillaceous limestone and soil which result in poor infiltration rates, greater runoff, and increased soil moisture storage and thus more water can be used to meet evaporative demand (Gingerich, 2010; Johnson, 2012).

4.2. Scaling Behavior

The scaling behavior observed in the frequency domain (Figure 4) reflects the nonlinear connection of energy from high to low frequency (Zhang & Li, 2005; Zhang & Schilling, 2004). The $1/f^{\alpha}$ scaling behavior characterizes many natural phenomena but not all scaling behaviors are fully understood (Kirchner et al., 2000; Yu et al., 2016). At low frequencies, the dominating factor driving response of the system is matrix storage. This flatter behavior, or hill and plateau, indicates that the transfer of energy is dominated by internal processes and characteristics, that is, storage and permeability. Recall the transfer function is recharge to precipitation, and thus higher values in this range of the transfer function indicates continued groundwater inputs as precipitation goes to zero. The higher frequencies, which are also flatlined, are dominated by external stressors such as precipitation. Spectral density plots for precipitation can indeed be considered a white noise process with characteristic flat spectrogram (Vasseur & Yodzis, 2004) and as such, the frequency spectra of the transfer function and recharge mimics the

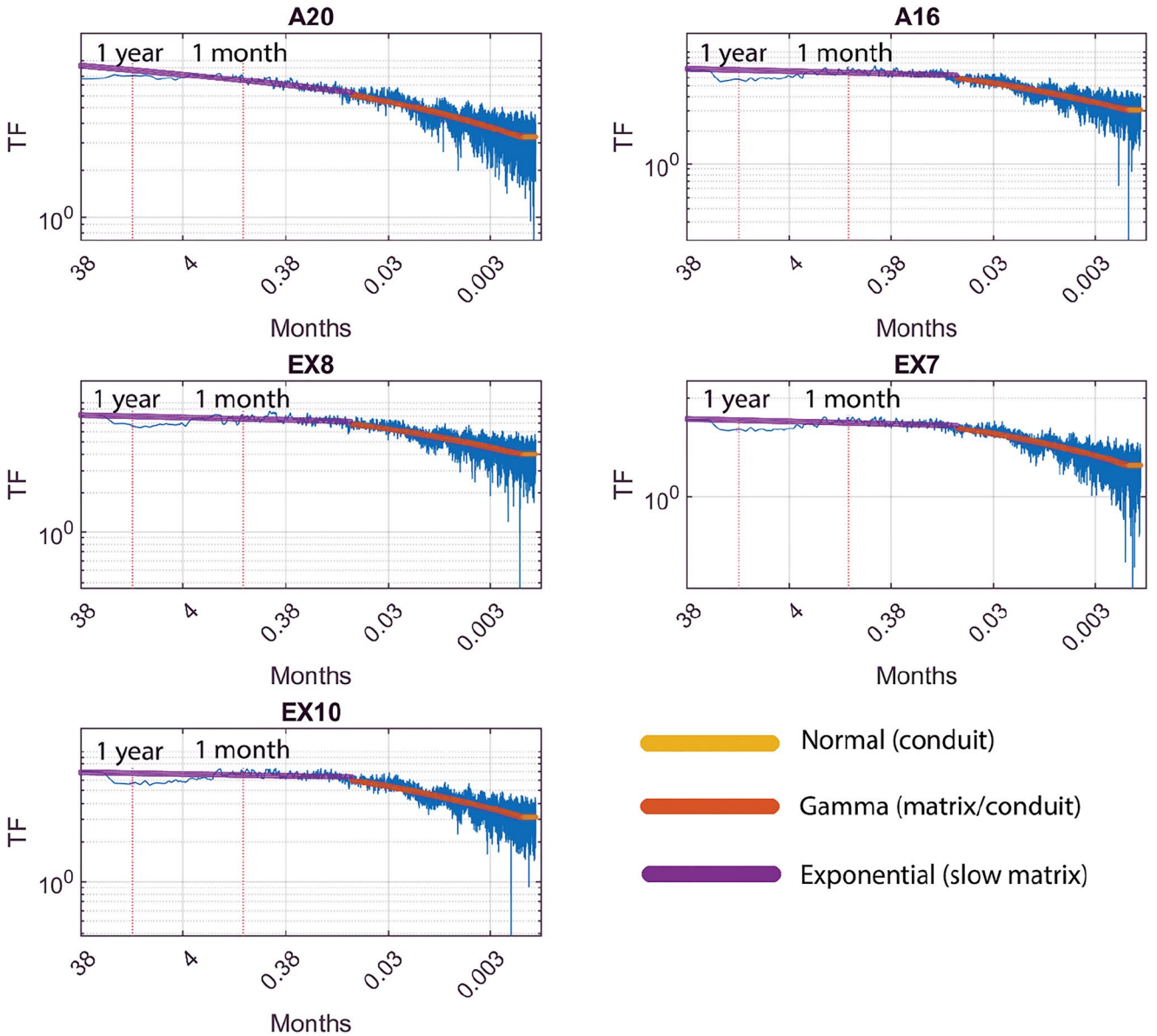

Figure 4. For each well, the total estimated transfer function and distribution fits are shown. Colored lines correspond to different fitted probability distributions for each partitioned reservoir.

white noise process as water flows through the high permeability pathways with little resistance. The mid-level frequencies are where the scaling behavior is observed, and this likely represents combination effect of external and internal non-linear processes (Godsey et al., 2010; Kirchner et al., 2000). The sloping behavior of the transfer function power spectra for matrix/conduit flow indicates the contribution of a slowly draining storage reservoir which is dependent upon the previous internal state of the system. As rainfall on Guam can occur daily, particularly in the wet season, and can last longer than the conduit estimated flow travel times (~1.5 hr), the saturation state of the system begins to play a role, whereby nonlinear interactive processes of saturated flow, evapotranspiration, movement through the soil zone, and continued rainfall combine to produce the $1/f^{\alpha}$ scaling behavior. Over the analyzed time span, the combination of these processes likely contributed to the range in travel times observed.

The use of these methods with non-stationary data should be cautioned, as lower frequency oscillations (e.g., El Nino) may be picked up if not acknowledged or filtered out. The data used for this analysis was tested for non-stationarity and kept to a relatively small sample (5-year) which avoided such complications. Seasonal

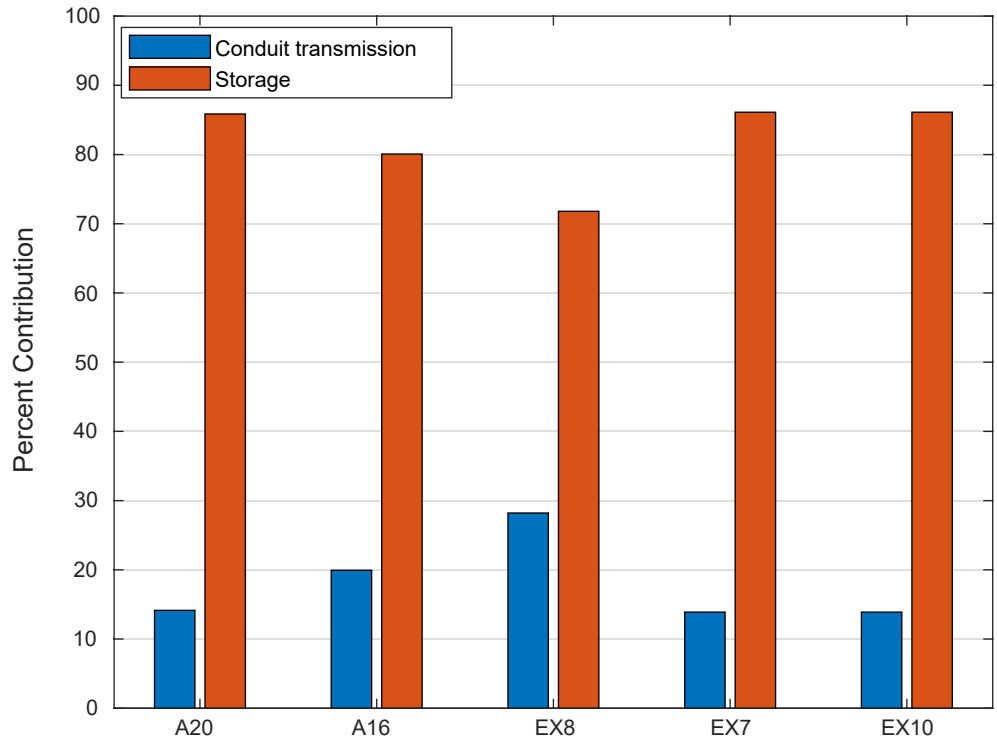

Figure 5. Average percent contributions from storage and fast flow at each well.

effects may also be apparent in the low-frequency region, but the signal in this analysis did not significantly change from the flatlined behavior after the scaling effect ceased (Figure 4). For regions with significant seasonal changes however, this should be considered when performing these analyses.

Typhoons and tropical storms, commonly impacting Guam, could potentially bias the responses in the data set. However, no typhoons or significant tropical systems made landfall during the 5-year period of analysis, and therefore our data set captures typical tropical rainfall patterns observed on Guam. The introduction of significant rainfall from a typhoon could cause substantial vadose flushing during an event and potentially move significant volumes of stored water through the vadose zone which could convolute the conduit flow dynamics interpreted herein. Therefore, further analyses uniquely identifying the effect of substantial rainfall from typhoons on vadose storage and subsequent aquifer recharge is warranted.

Though wells near highly urbanized areas were avoided to reduce the influence of stormwater routing and pumping, the small size of the island and its karstic nature raise the possibility that pumping effects may be present in the groundwater data. The influence that pumping has on the estimated transfer function behavior has not been thoroughly investigated, however, one study in a fractured karst aquifer showed that the slopes of the transfer function were shallower at mid to high frequencies where pumping was prevalent and sharp, discernible breaks occurred that created nonlinearities of the transfer function in log-log space (Jimenez-Martinez et al., 2013). Shallower slopes would produce slower travel times than determined in our analysis for mid to high frequencies, and therefore if any of our wells had influence from pumping, our travel time estimates would be slower than reported. However, no discernible breaks occurred in the transfer function that were similar to those observed in other studies where pumping was known to be affecting water levels, and therefore, we assume that the effects pumping would have on our results would be minimal.

4.3. Partitioning of Discrete Versus Diffuse Flow

The choice to use complementary methods for the component partitioning comes from a desire to validate mathematical methods to physically based ones. By estimating the divergence from white noise to partition conduit and the matrix/conduit flow, the assumed process is maintained with a mathematical basis. Taking the inflection

point indicates that there is a change in curvature of the function (herein fitted as a sixth degree polynomial), and thus the response when the slope of the curve is flatter is assumed to be a longer-term storage component. However, because the inflection point is dependent upon the polynomial fit, it can lead to some error and bias. For this reason, more physically based methods were also used as validation. Both methods produced similar results for each break (conduit to matrix/conduit and matrix/conduit to matrix), which was verified by visual means. However, the frequency identified by the inflection point of the polynomial at the matrix/conduit to matrix partition presented a visually more reasonable partition, likely due to a slight slope maintained in the matrix only component.

One assumption behind the component partitions is that there is no matrix flow in the initial period and that storage dominates the transition to matrix/conduit flow. That is likely not the case, as the instantaneous pressure pulse from precipitation can move water out of storage, indicating that some recharged water may not have been from the impulse event (Covington et al., 2009). The water moved out of storage causing a rapid groundwater response is possibly pushed into conduits and moved through the fast flow pathways. Though the distinction is subtle, it affects interpretation and assumptions on flow through the vadose zone, whereby infiltration that causes a response may not be from the contemporaneous storm event (Kirchner, 2003). Thus, the age of the water may be different and cannot be discerned completely with the methods utilized in this study. This also has implications for magnitude scaling, as precipitation and recharge will likely not have a linear response function. Additional error in recharge estimates based on MRC curves can also occur, as recession behavior is not guaranteed to be free from slow, percolating recharge. In the case of MRC curves, we may expect some slow percolation during a captured recession, which could underestimate possible recharge values as it would possibly reduce the value the fitted recession constant. Furthermore, there are likely conduit contributions that occur after the transition period as water moves out of storage via gravitational forces and contributes to groundwater recharge. However, this is likely balanced by movement out of matrix storage through gravitational forces and head changes and therefore, is still reflective of storage in the vadose zone. Though we recognize this process, we emphasize that our work is the first step to understand the timescales of movement through the vadose zone via different flow pathways. We also suggest that more work parsing out unique event-based signals would improve the analysis, including additional hydrological modeling and geochemical sampling at key locations to understand water ages.

The decision to partition flow into matrix/conduit and long-term matrix components was done because of mathematical changes that led to an interpretive process control. The break in slope, whereby the scaling behavior flatlines, made fitting a continuous distribution challenging. Therefore, the break was determined via polynomial function analysis and an additional distribution was fit to the flatlined storage. The flatline suggests that recharge beyond that inflection point is a steady flow rate that continues in the absence of any precipitation. The slight decrease at the lower frequencies suggests that stored water contributing to recharge does eventually decrease.

The estimated travel times fitted for storage cannot be considered firm estimates due to the constrained data set. Water in the long-term matrix storage may take several years to travel through the vadose zone (Jones & Banner, 2003; Lander, 1994; Partin et al., 2012; Vacher & Wallis, 1992) and as such, a larger data set is needed. Our data however was restricted to the long-term continuous data set that existed and additional long-term, high resolution monitoring may be warranted to fully understand decadal scale climatic effects. However, the median travel time estimated from the fitted power law for longer term storage indicated that around ~80% recharged the NGLA in just over a month. Therefore, it may be assumed that the subsequent contributions that occur from the matrix may be minimal compared to the overall infiltrated water, albeit measurable.

Previous studies estimating flow through the unsaturated zone have shown wide ranges in estimated time in storage. Timescales of fast flow through a rock pile showed preferential pathways taking 2 days to move through the five-m high, experimental rock pile (Trinchero et al., 2011). The methods used to estimate the travel flow times through the experimental setup were similar in the Guam vadose system, however they used a large boulder rock pile which inherently has tortuous and smaller pathways of flow than in the vadose zone in Guam, which likely has a significant number of vertical fractures and conduits. Our timescales are smaller than timescales observed for fast flow within the rock pile, which may be due the difference in partitioning slow versus fast pathways as well as large conduits that likely exist which can transmit water faster.

Though the vadose zone shows clear controls on the timing of recharge delivery, implementing contributions from this zone in groundwater modeling on Guam has been challenging. The first groundwater model that incorporated

the importance of vadose storage used a direct infiltration value of 33% of daily averaged precipitation to immediately recharge the water table for all events (Contractor & Jenson, 2000). Though model performance improved over not considering storage at all, significant error between observed and simulated values remained. For the same model, a range of days were observed for significant delays between precipitation and groundwater response, indicating that other factors such as precipitation intensity, evapotranspiration and antecedent vadose storage may affect recharge timing and a single value may be inadequate. Our estimates of 12%–28% of conduit flow contributions conform to the previously attempted methods used to improve daily groundwater level fluctuation performance on Guam. Though the contributions estimated for recharge are based on the overall recharge and precipitation estimates for the time period analyzed, it is not unreasonable to assume the similar contribution at the event scale from each component. Further analyses on recharge thresholds and how recharge threshold variability may change in the wet and dry season would also improve hydrological model efforts.

5. Conclusions

We reported a comprehensive analysis of recharge and recharge dynamics for a karst aquifer that has a thick vadose zone. We used legacy data and a modification of the WTF method to estimate recharge in the time domain. Our recharge aligned with previous data, not only providing confidence in recharge estimates, but also confirming the efficacy of the WTF method for deep, karstic water tables which had not previously been done. We developed a method to partition conduit and matrix components of the vadose zone and estimated the average travel times of water through each of the components by fitting probability distributions to transfer functions developed in the frequency domain.

Our analysis of the developed transfer functions shows that most of the recharge in Guam occurs relatively quickly, with >70% occurring within a month. These results illustrate that although most water recharges the aquifer within a month of a precipitation event, storage can be appreciable in a karstic vadose zone. The methods developed can quantify storage in eogenetic and telogenetic systems which can be used to improve hydrological modeling on timescales needed for karst aquifer management.

Data Availability Statement

All data, including MATLAB codes, are freely available at HydroShare (http://www.hydroshare.org/resource/ea9e33869083476 39adb1946cd85f60d).

Acknowledgments
The authors would like to thank the anonymous reviewers who made valuable comments to significantly improve the manuscript.

References

Abusaada, M., & Sauter. (2019). Recharge estimation in karst aquifers by applying water level fluctuation approach. *International Journal of Earth Science and Geophysics*, *3*(1). https://doi.org/10.35840/2631-5033/1813

Bailly-Comte, V., Jourde, H., Roesch, A., Pistre, S., & Batiot-Guilhe, C. (2008). Time series analyses for Karst/River interactions assessment: Case of the Coulazou River (southern France). *Journal of Hydrology*, *349*(1–2), 98–114. https://doi.org/10.1016/j.jhydrol.2007.10.028

Bailly-Comte, V., Martin, J. B., Jourde, H., Screaton, E. J., Pistre, S., & Langston, A. (2010). Water exchange and pressure transfer between conduits and matrix and their influence on hydrodynamics of two karst aquifers with sinking streams. *Journal of Hydrology*, *386*(1–4), 55–66. https://doi.org/10.1016/j.jhydrol.2010.03.005

Batiot, C., Liñán, C., Andreo, B., Emblanch, C., Carrasco, F., & Blavoux, B. (2003). Use of Total Organic Carbon (TOC) as tracer of diffuse infiltration in a dolomitic karstic system: The Nerja Cave (Andalusia, southern Spain). *Geophysical Research Letters*, *30*(22), 2179. https://doi.org/10.1029/2003gl018546

Bautista, K. K., Jenson, J. W., Lander, M. A., & Righetti, T. (2018). Vadose hydrology at Jinapsan cave, Northern Guam. *Water and Environmental Research Institute of the Western Pacific Technical Reports*, *163*.

Beal, L. K., Wong, C. I., Bautista, K. K., Jenson, J. W., Banner, J. L., Lander, M. A., et al. (2019). Isotopic and geochemical assessment of the sensitivity of groundwater resources of Guam, Mariana Islands, to intra-and inter-annual variations in hydroclimate. *Journal of Hydrology*, *568*, 174–183. https://doi.org/10.1016/j.jhydrol.2018.10.049

Beddows, P. A., & Mallon, E. K. (2018). Cave pearl data logger: A flexible arduino-based logging platform for long-term monitoring in harsh environments. *Sensors*, *18*(2), 530. https://doi.org/10.3390/s18020530

Besbes, M., & De Marsily, G. (1984). From infiltration to recharge: Use of a parametric transfer function. *Journal of Hydrology*, *74*(3–4), 271–293. https://doi.org/10.1016/0022-1694(84)90019-2

Bonacci, O. (1988). 'Determination of the catchment areas in karst'. In *Karst hydrogeology and karst environment protection, 21st congres of IAH* (Vol. XXI, pp. 606–611). Proceedings, Geological Publ. House.

Bonacci, O. (1993). Karst springs hydrographs as indicators of karst aquifers. *Hydrological Sciences Journal*, *38*(1), 51–62. https://doi.org/10.1080/02626669309492639

Breithaupt, C. I., Gulley, J. D., Moore, P. J., Fullmer, S. M., Kerans, C., & Mejia, J. Z. (2021). Flank margin caves can connect to regionally extensive touching vug networks before burial: Implications for cave formation and fluid flow. *Earth Surface Processes and Landforms*, *46*(8), 1458–1481. https://doi.org/10.1002/esp.5114

Bronez, T. P. (1992). On the performance advantage of multitaper spectral analysis. *IEEE Transactions on Signal Processing*, *40*(12), 2941–2946. https://doi.org/10.1109/78.175738

Budd, D. A., & Vacher, H. L. (1991). Predicting the thickness of fresh-water lenses in carbonate paleo-islands. *Journal of Sedimentary Research*, *61*(1), 43–53.

Caballero, E., De Cisneros, C. J., & Reyes, E. (1996). A stable isotope study of cave seepage waters. *Applied Geochemistry*, *11*(4), 583–587. https://doi.org/10.1016/0883-2927(96)00026-1

Chapman, J. B., Ingraham, N. L., & Hess, J. W. (1992). Isotopic investigation of infiltration and unsaturated zone flow processes at Carlsbad Cavern, New Mexico. *Journal of Hydrology*, *133*(3–4), 343–363. https://doi.org/10.1016/0022-1694(92)90262-t

Chen, Q., Chang, H., Govindan, R., & Jamin, S. (2002). The origin of power laws in Internet topologies revisited. In *Proceedings. twenty-first annual joint conference of the IEEE computer and communications societies* (Vol. 2, pp. 608–617). IEEE.

Choquette, P. W., & Pray, L. C. (1970). Geologic nomenclature and classification of porosity in sedimentary carbonates. *AAPG Bulletin*, *54*(2), 207–250.

Contractor, D. N., & Jenson, J. W. (2000). Simulated effect of vadose infiltration on water levels in the Northern Guam Lens Aquifer. *Journal of Hydrology*, *229*(3–4), 232–254. https://doi.org/10.1016/s0022-1694(00)00157-8

Covington, M. D., Wicks, C. M., & Saar, M. O. (2009). A dimensionless number describing the effects of recharge and geometry on discharge from simple karstic aquifers. *Water Resources Research*, *45*(11), W11410. https://doi.org/10.1029/2009wr008004

Crosbie, R. S., Binning, P., & Kalma, J. D. (2005). A time series approach to inferring groundwater recharge using the water table fluctuation method. *Water Resources Research*, *41*(1), W01008. https://doi.org/10.1029/2004WR003077

Dyck, M. F., Kachanoski, R. G., & De Jong, E. (2005). Spatial variability of long-term chloride transport under semiarid conditions: Pedon scale. *Vadose Zone Journal*, *4*(4), 915–923. https://doi.org/10.2136/vzj2004.0162

Emblanch, C., Zuppi, G. M., Mudry, J., Blavoux, B., & Batiot, C. (2003). Carbon 13 of TDIC to quantify the role of the unsaturated zone: The example of the Vaucluse karst systems (Southeastern France). *Journal of Hydrology*, *279*(1–4), 262–274. https://doi.org/10.1016/s0022-1694(03)00180-x

Engott, J. A. (2011). *A water-budget model and assessment of groundwater recharge for the Island of Hawai 'i: USGS scientific investigations report 2011-5078*. US Geological Survey.

Ferris, J. G. (1951). *Cyclic fluctuations of water level as a basis for determining aquifer transmissibility (No. Note 1)*. US Geological Survey.

Florea, L. J., & Vacher, H. L. (2005). Springflow hydrographs: Eogenetic vs. telogenetic karst. *Groundwater*, *44*(3), 352–361. https://doi.org/10.1111/j.1745-6584.2005.00158.x

Florea, L. J., & Vacher, H. L. (2006). Springflow hydrographs: Eogenetic vs. telogenetic karst. *Groundwater*, *44*(3), 352–361. https://doi.org/10.1111/j.1745-6584.2005.00158.x

Florea, L. J., & Vacher, H. L. (2007). Eogenetic karst hydrology: Insights from the 2004 hurricanes, peninsular Florida. *Groundwater*, *45*(4), 439–446. https://doi.org/10.1111/j.1745-6584.2007.00309.x

Ford, D., & Williams, P. D. (2013). *Karst hydrogeology and geomorphology*. John Wiley & Sons.

Garry, B., Blondel, T., Emblanch, C., Sudre, C., Bilgot, S., Cavaillou, A., et al. (2008). Contribution of artificial galleries to knowledge of karstic system behaviour in addition to natural cavern data. *International Journal of Speleology*, *37*(1), 75–82. https://doi.org/10.5038/1827-806x.37.1.7

Gingerich, S. B. (2010). Hydrologic resources of Guam: US geological Survey water-resources investigations report 03-4126, 2 plates. Accessibility FOIA Privacy Policies and Notices US Department of the Interior. *US Geological Survey Persistent URL: Page Contact Information: Contact USGS Last modified: Friday*, *4*, 03–34.

Gingerich, S. B. (2013). *The effects of withdrawals and drought on groundwater availability in the Northern Guam Lens Aquifer, Guam*. US Geological Survey Scientific Investigations Report.

Godsey, S. E., Aas, W., Clair, T. A., De Wit, H. A., Fernandez, I. J., Kahl, J. S., et al. (2010). Generality of fractal 1/f scaling in catchment tracer time series, and its implications for catchment travel time distributions. *Hydrological Processes*, *24*(12), 1660–1671. https://doi.org/10.1002/hyp.7677

Habana, N. C., Heitz, L. F., Olsen, A. E., Jenson, J. W., & Salvacion, J. L. (2013). VADOCHARGE: Groundwater recharge model for an uplifted Island karst aquifer, Guam, USA. *International Journal of Environmental Engineering Science and Technology Research*, *1*(8), 141–164.

Harmon, R. S. (1979). An isotopic study of groundwater seepage in the central Kentucky karst. *Water Resources Research*, *15*(2), 476–480. https://doi.org/10.1029/wr015i002p00476

Healy, R. W., & Cook, P. G. (2002). Using groundwater levels to estimate recharge. *Hydrogeology Journal*, *10*(1), 91–109. https://doi.org/10.1007/s10040-001-0178-0

Izuka, S. K., Oki, D. S., & Engott, J. A. (2010). Simple method for estimating groundwater recharge on tropical islands. *Journal of Hydrology*, *387*(1–2), 81–89. https://doi.org/10.1016/j.jhydrol.2010.03.034

Jackson, J. A. (1997). In *Glossary of geology* (Vol. 11, pp. 999–1012). American Geological Institute.

Jiménez-Martínez, J., Longuevergne, L., Le Borgne, T., Davy, P., Russian, A., & Bour, O. (2013). Temporal and spatial scaling of hydraulic response to recharge in fractured aquifers: Insights from a frequency domain analysis. *Water Resources Research*, *49*(5), 3007–3023. https://doi.org/10.1002/wrcr.20260

Jocson, J. M. U., Jenson, J. W., & Contractor, D. N. (2002). Recharge and aquifer response: Northern Guam lens aquifer, Guam, Mariana Islands. *Journal of Hydrology*, *260*(1–4), 231–254. https://doi.org/10.1016/s0022-1694(01)00617-5

Johnson, A. G. (2012). A water-budget model and estimates of groundwater recharge for Guam. *US Geological Survey Scientific Investigations Report*, *5028*, 00346–00348.

Jones, I. C., & Banner, J. L. (2003). Estimating recharge thresholds in tropical karst island aquifers: Barbados, Puerto Rico and Guam. *Journal of Hydrology*, *278*(1–4), 131–143. https://doi.org/10.1016/s0022-1694(03)00138-0

Jones, I. C., Banner, J. L., & Humphrey, J. D. (2000). Estimating recharge in a tropical karst aquifer. *Water Resources Research*, *36*(5), 1289–1299. https://doi.org/10.1029/1999wr900358

Jukić, D., & Denić-Jukić, V. (2004). A frequency domain approach to groundwater recharge estimation in karst. *Journal of Hydrology*, *289*(1–4), 95–110. https://doi.org/10.1016/j.jhydrol.2003.11.005

Kirchner, J. W. (2003). A double paradox in catchment hydrology and geochemistry. *Hydrological Processes*, *17*(4), 871–874. https://doi.org/10.1002/hyp.5108

Kirchner, J. W. (2005). Aliasing in 1/ f α noise spectra: Origins, consequences, and remedies. *Physical Review E*, *71*(6), 066110. https://doi.org/10.1103/physreve.71.066110

Kirchner, J. W., Feng, X., & Neal, C. (2000). Fractal stream chemistry and its implications for contaminant transport in catchments. *Nature*, *403*(6769), 524–527. https://doi.org/10.1038/35000537

Kirchner, J. W., & Neal, C. (2013). Universal fractal scaling in stream chemistry and its implications for solute transport and water quality trend detection. *Proceedings of the National Academy of Sciences*, *110*(30), 12213–12218. https://doi.org/10.1073/pnas.1304328110
Kogovšek, J. (1997). Water tracing tests in vadose zone. *Tracer hydrology*, *97*, 167–172.
Lander, M. A. (1994). In *Meteorological factors associated with drought on Guam. Technical Report* (Vol. 75). Water and Environment Research Institute.
Larocque, M., Mangin, A., Razack, M., & Banton, O. (1998). Contribution of correlation and spectral analyses to the regional study of a large karst aquifer (Charente, France). *Journal of Hydrology*, *205*(3–4), 217–231. https://doi.org/10.1016/s0022-1694(97)00155-8
Lases-Hernandez, F., Medina-Elizalde, M., Burns, S., & DeCesare, M. (2019). Long-term monitoring of drip water and groundwater stable isotopic variability in the Yucatán Peninsula: Implications for recharge and speleothem rainfall reconstruction. *Geochimica et Cosmochimica Acta*, *246*, 41–59. https://doi.org/10.1016/j.gca.2018.11.028
Maillet, E. T. (1905). *Tests of underground & river hydraulics*. A. Hermann.
Mink, J. F. (1976). *GroundwaterresourcesonGuam:occurrenceanddevelopment. Technical report No. 1, water and EnergyResearch Institute of the Western Pacific*. University of Guam.
Mink, J. F., & Vacher, H. L. (1997). Hydrogeology of northern Guam. In H. L. Vacher & T. Quinn (Eds.), *GeologyandHydrogeologyof carbonate Islands. Developments in sedimentology 54Else-vier* (pp. 743–761).
Molénat, J., Davy, P., Gascuel-Odoux, C., & Durand, P. (1999). Study of three subsurface hydrologic systems based on spectral and cross-spectral analysis of time series. *Journal of Hydrology*, *222*(1–4), 152–164. https://doi.org/10.1016/s0022-1694(99)00107-9
Moore, P. J., Martin, J. B., Screaton, E. J., & Neuhoff, P. S. (2010). Conduit enlargement in an eogenetic karst aquifer. *Journal of Hydrology*, *393*(3–4), 143–155. https://doi.org/10.1016/j.jhydrol.2010.08.008
Padilla, A., & Pulido-Bosch, A. (1995). Study of hydrographs of karstic aquifers by means of correlation and cross-spectral analysis. *Journal of Hydrology*, *168*(1–4), 73–89. https://doi.org/10.1016/0022-1694(94)02648-u
Pagendam, D. E., & Percival, D. B. (2015). Estimating freshwater flows from tidally affected hydrographic data. *Water Resources Research*, *51*(3), 1619–1634. https://doi.org/10.1002/2014wr015706
Panagopoulos, G., & Lambrakis, N. (2006). The contribution of time series analysis to the study of the hydrodynamic characteristics of the karst systems: Application on two typical karst aquifers of Greece (Trifilia, Almyros Crete). *Journal of Hydrology*, *329*(3–4), 368–376. https://doi.org/10.1016/j.jhydrol.2006.02.023
Partin, J. W., Jenson, J. W., Banner, J. L., Quinn, T. M., Taylor, F. W., Sinclair, D., et al. (2012). Relationship between modern rainfall variability, cave dripwater, and stalagmite geochemistry in Guam, USA. *Geochemistry, Geophysics, Geosystems*, *13*(3), Q03013. https://doi.org/10.1029/2011gc003930
Perrin, J., Jeannin, P. Y., & Zwahlen, F. (2003). Epikarst storage in a karst aquifer: A conceptual model based on isotopic data, Milandre test site, Switzerland. *Journal of Hydrology*, *279*(1–4), 106–124. https://doi.org/10.1016/s0022-1694(03)00171-9
Pishro-Nik, H. (2016). Introduction to probability, statistics, and random processes.
Poulain, A., Watlet, A., Kaufmann, O., Van Camp, M., Jourde, H., Mazzilli, N., et al. (2018). Assessment of groundwater recharge processes through karst vadose zone by cave percolation monitoring. *Hydrological Processes*, *32*(13), 2069–2083. https://doi.org/10.1002/hyp.13138
Prieto, G. A., Parker, R. L., Thomson, D. J., Vernon, F. L., & Graham, R. L. (2007). Reducing the bias of multitaper spectrum estimates. *Geophysical Journal International*, *171*(3), 1269–1281. https://doi.org/10.1111/j.1365-246x.2007.03592.x
Rimon, Y., Dahan, O., Nativ, R., & Geyer, S. (2007). Water percolation through the deep vadose zone and groundwater recharge: Preliminary results based on a new vadose zone monitoring system. *Water Resources Research*, *43*(5), W05402. https://doi.org/10.1029/2006wr004855
Risser, D. W., Gburek, W. J., & Folmar, G. J. (2005). *Comparison of methods for estimating ground-water recharge and base flow at a small watershed underlain by fractured bedrock in the Eastern United States* (pp. 2005–5038). US Geological Survey Scientific Investigation Report.
Rotzoll, K., Gingerich, S. B., Jenson, J. W., & El-Kadi, A. I. (2013). Estimating hydraulic properties from tidal attenuation in the Northern Guam Lens Aquifer, territory of Guam, USA. *Hydrogeology Journal*, *21*(3), 643–654. https://doi.org/10.1007/s10040-012-0949-9
Shirahata, K., Yoshimoto, S., Tsuchihara, T., & Ishida, S. (2016). Digital filters to eliminate or separate tidal components in groundwater observation time-series data. *Japan Agricultural Research Quarterly: JARQ*, *50*(3), 241–252. https://doi.org/10.6090/jarq.50.241
Smart, P. L., & Friederich, H. (1986). Water movement and storage in the unsaturated zone of a maturely karstified carbonate aquifer, Mendip Hills, England. In *Proceedings of the environmental problems in karst terranes and their solutions conference* (pp. 59–87). National Water Well Association. 11 fig, 5 tab, 38 ref.
Thomson, D. J. (1982). Spectrum estimation and harmonic analysis. *Proceedings of the IEEE*, *70*(9), 1055–1096. https://doi.org/10.1109/proc.1982.12433
Thrailkill, J. (1968). Chemical and hydrologic factors in the excavation of limestone caves. *The Geological Society of America Bulletin*, *79*(1), 19–46. https://doi.org/10.1130/0016-7606(1968)79[19:cahfit]2.0.co;2
Toebes, C., & Strang, D. D. (1964). On recession curves, 1. *Recession equations: Journal of Hydrology (New Zealand)*, *3*(2), 2–14.
Tracy, J. J. I., Stensland, C. H., Doan, D. B., May, H. G., Schlanger, S. O., & Stark, J. T. (1959). *Military geology of Guam, Mariana Islands. Part I. Description of terrain and environment. Part II. Engineering aspects of geology and soils*. Intelligence Division, Office of the Engineer, United States Army of the Pacific.
Trinchero, P., Beckie, R., Sanchez-Vila, X., & Nichol, C. (2011). Assessing preferential flow through an unsaturated waste rock pile using spectral analysis. *Water Resources Research*, *47*(7). https://doi.org/10.1029/2010wr010163
Vacher, H. L., & Ayers, J. F. (1980). Hydrology of small oceanic islands—Utility of an estimate of recharge inferred from the chloride concentration of the freshwater lenses. *Journal of Hydrology*, *45*(1–2), 21–37. https://doi.org/10.1016/0022-1694(80)90003-7
Vacher, H. L., Bengtsson, T. O., & Plummer, L. N. (1990). Hydrology of meteoric diagenesis: Residence time of meteoric ground water in island fresh-water lenses with application to aragonite-calcite stabilization rate in Bermuda. *The Geological Society of America Bulletin*, *102*(2), 223–232. https://doi.org/10.1130/0016-7606(1990)102<0223:homdrt>2.3.co;2
Vacher, H. L., & Mylroie, J. E. (2002). Eogenetic karst from the perspective of an equivalent porous medium. *Carbonates and Evaporites*, *17*(2), 182–196. https://doi.org/10.1007/bf03176484
Vacher, H. L., & Wallis, T. N. (1992). Comparative hydrogeology of fresh-water lenses of Bermuda and Great Exuma Island, Bahamas. *Groundwater*, *30*(1), 15–20. https://doi.org/10.1111/j.1745-6584.1992.tb00806.x
Vasseur, D. A., & Yodzis, P. (2004). The color of environmental noise. *Ecology*, *85*(4), 1146–1152. https://doi.org/10.1890/02-3122
Veni, G. (1999). A geomorphological strategy for conducting environmental impact assessments in karst areas. *Geomorphology*, *31*(1–4), 151–180. https://doi.org/10.1016/s0169-555x(99)00077-x
Walters, R. A., & Heston, C. (1982). Removing tidal-period variations from time-series data using low-pass digital filters. *Journal of Physical Oceanography*, *12*(1), 112–115. https://doi.org/10.1175/1520-0485(1982)012<0112:rtpvft>2.0.co;2

Williams, P. W. (2008). The role of the epikarst in karst and cave hydrogeology: A review. *International Journal of Speleology*, *37*(1), 1–10. https://doi.org/10.5038/1827-806x.37.1.1

Worthington, S. R. (2019). How preferential flow delivers pre-event groundwater rapidly to streams. *Hydrological Processes*, *33*(17), 2373–2380. https://doi.org/10.1002/hyp.13520

Yu, X., Ghasemizadeh, R., Padilla, I. Y., Kaeli, D., & Alshawabkeh, A. (2016). Patterns of temporal scaling of groundwater level fluctuation. *Journal of Hydrology*, *536*, 485–495. https://doi.org/10.1016/j.jhydrol.2016.03.018

Zhang, Y. K., & Li, Z. (2005). Temporal scaling of hydraulic head fluctuations: Nonstationary spectral analyses and numerical simulations. *Water Resources Research*, *41*(7). https://doi.org/10.1029/2004wr003797

Zhang, Y. K., & Schilling, K. (2004). Temporal scaling of hydraulic head and river base flow and its implication for groundwater recharge. *Water Resources Research*, *40*(3). https://doi.org/10.1029/2003wr002094